Infrared Reflection Absorption Spectroscopic and DFT Calculation Studies on the Adsorption Structures of Dimethyl Ether on Ag(110), Cu(110), and Their Atomic Oxygen-Reconstructed Surfaces†

Tairiku Kiyohara, Masato Akita, Chikaomi Ohe, and Koichi Itoh*

Department of Chemistry, School of Science and Engineering,Waseda University, Shinjuku-ku, Tokyo 169-8555, Japan

Received: July 11, 2001

Infrared spectra were measured at 80 K for dimethyl ether (CH_3OCH_3, DME) and dimethyl ether-d_6 (CD_3OCD_3, DME-d_6) with increasing amounts of exposures to metal substrates, Ag(110), Cu(110), and their atomic oxygen-reconstructed surfaces, p(2 × 1)O−Ag(110) and p(2 × 1)O−Cu(110). At relatively lower surface coverages, the IR spectra of DME on Ag(110) and Cu(110) in the 1500−800 cm^{-1} region give rise to IR bands mainly ascribable to A_1 species, including symmetric COC stretching (ν_s(COC)) bands at 903 cm^{-1} on Ag(110) and 895 cm^{-1} on Cu(110), while at nearly saturation coverages, the adsorbate gives IR bands ascribable to B_1 and/or B_2 species in addition to the A_1 bands with the ν_s(COC) band discretely sifted to 915 cm^{-1} on Ag(110) and to 901 cm^{-1} on Cu(110). Similar distinct spectral changes were observed also for DME and DME-d_6 on the reconstructed surfaces. The stepwise spectral changes were interpreted in terms of a conversion from a state of DME with the C_2 axis almost perpendicular to the surfaces to a state with the C_2 axis tilted away from the perpendicular orientation. Fermi resonance effects cause stepwise but complicated spectral changes in the CH_3 stretching vibration region of DME during the conversion. The changes strongly depend on the kind of the substrates, in contrast to the spectral changes in the 1500−800 cm^{-1} region, suggesting that the analyses of Fermi resonances can delineate subtle differences in the DME/substrate interaction modes among the substrates. Density functional theory (DFT) molecular orbital calculations were carried out on the cluster models of DME/Cu(110), where the oxygen atom of DME is coordinated to two copper atoms in the surface of metal clusters consisting of 12 copper atoms in the first layer and six copper atoms in the second layer. The results of calculations reproduce the observed frequencies appreciably well, substantiating the coordination interaction model.

Introduction

Infrared reflection absorption spectroscopy (IRAS) has been established as one of the most powerful methods to elucidate the structures, adsorbate/substrate interactions and reaction processes of adsorbates on various metal surfaces.[1−3] We have applied this method to study the adsorption processes of simple organic molecules containing C═C bonds such as acrolein,[4] 1,3-butadiene,[5] acrylonitrile,[6] and ethylene[7] adsorbed on relatively inert metals such as silver and gold; the frequency shifts and intensity changes as well as splitting of IR bands observed for the adsorbates with increasing surface coverages have been interpreted in terms of a weak π-bonding interaction of the C═C bond, changes in adsorption states and sites, and an association dissociation equlibrium of the adsorbates on the surfaces. As an extension of these studies, we applied IRAS in this paper to elucidate the adsorption characteristics of dimethyl ether (CH_3OCH_3, DME) and dimethyl ether-d_6(CD_3OCD_3, DME-d_6) on Ag(110), Cu(110), and their atomic oxygen-reconstructed surfaces, p(2 × 1)-O−Ag(110) and p(2 × 1)-O−Cu(110). The points to be clarified by this paper are as follows: (i) the surface coverage dependence of the structure, orientations, and adsorption sites of DME on the substrates, (ii) the participation of coordination of the oxygen atom of DME to the silver and copper atoms in the adsorbate/substrate interaction, (iii) the differences in the interaction among Cu(110), Ag(110) and their atomic oxygen-reconstructed surfaces, (iv) the effects of Fermi resonances between the CH_3 stretching fundamental modes and the overtone and/or combination modes of the CH_3 deformation vibrations on the spectra of the adsorbed DME in the CH_3 stretching vibration region, where subtle changes in the frequencies of the CH_3 stretching and deformation fundamental modes may cause enhanced spectral changes through the resonances, and (v) the validity of performing molecular orbital calculations based on the density functional theory (DFT) for cluster models of DME/Cu(110) for the analysis of the observed spectra.

The IR and Raman spectra of DME and DME-d_6 have already been reported,[8−10] and ab initio molecular orbital calculations of vibrational frequencies have been performed on DME by McKean et al.[11] As for DME on metal surfaces, Sexton and Hughes[12] performed temperature-programmed desorption (TPD) and spectroscopic studies on the adsorbate on Cu(100), indicating the existence of two phases, i.e., a weakly bound monolayer phase with a desorption temperature (T_d) of 150 K and a multiplayer or condensed phase with T_d = 100 K. The high-resolution electron energy loss spectroscopy (HREELS) has been

† Part of the special issue "Mitsuo Tasumi Festschrift".

* Corresponding author. E-mail: itohk@mn.waseda.ac.jp. Fax: 81 3 5273 2606.

10.1021/jp0126053 CCC: $22.00
Published on Web 12/13/2001

applied to DME on Al(111) and on Rh(111);[13,14] the results proved the existence of molecularly adsorbed DME on the surfaces at 90−100 K and the desorprtion of the adsorbate without any sign of decomposition at elevated temperatures (100−200 K). The IR spectra of DME adsorbed on metal surfaces have not been reported yet. As explained in the following, the observation and detailed analyses of the spectra give insights into the adsorption characteristics of DME on Ag(110), Cu(110), and their reconstructed surfaces.

Experimental Section

Materials. DME (99% purity) and DME-d_6 (98% purity) were purchased from Tokyo Kasei Kogyo Co., Ltd., and Aldrich Co., respectively. These samples were used without further purification.

Substrates. Ag(110) and Cu(110) single crystals (99.999%, 15 mm(ϕ) × 1 mm) were purchased from Techno Chemics, Inc. The surfaces of the crystals were cleaned by Ar^+ ion sputtering (0.7 μA cm^{-2}, 700 eV, 15 min at 600 K) and annealing at the same temperature. The reconstructed surfaces, p(2 × 1)O−Ag(110) and p(2 × 1)O−Cu(110), were prepared by exposing the cleaned surfaces to appropriate amounts of oxygen at room temperature.[7] The formation of the reconstructed surfaces were confirmed by observing the anticipated LEED patterns.

Measurement of IR Spectra. The IR spectral measurements were performed by the apparatus already explained.[7] The apparatus consists of a load-lock chamber and two ultrahigh vacuum chambers; one of the UHV chambers containing a four-grid retarding field AES/LEED optics, a quadrupole mass spectrometer and an Ar^+ ion sputtering unit was used for preparing the clean and reconstructed surfaces, and the other UHV chamber containing an Fourier transform IR spectrometer (Brucker model 66v/S) was used for IRAS measurements. The IR spectra were recorded at an incident angle of 80° with a liquid nitrogen cooled MCT detector. The base pressure of the two chambers was below 1×10^{-10} Torr. The temperature of the substrates was cooled to 80 K by liquid nitrogen. DME and DME-d_6 were dosed to the substrates precooled at 80 K through a 1/8 in. stainless tube by using a variable leak valve. The intensity of the IR bands of the adsorbates on Ag(110) was found to saturate at a certain level of exposure. Since the exact surface coverage was not determined, it was assumed that a saturation coverage is formed at this stage. As for DME and DME-d_6 on Cu(110), p(2 × 1)O−Ag(110), and p(2 × 1)O−Cu(110), it was found that the IR intensities of the adsorbates increase with exposures. However, the formation of multilayers was easily detected by observing IR bands ascribable to crystalline states. So it was assumed that the saturation coverage was completed just before the appearance of such bands. All the spectra were given by $-\log(R/R_0)$ as a function of wavenumber in the 4000−750 cm^{-1} region, where R and R_0 indicate measured reflection intensities with and without an adsorbate, respectively. Reflection intensities were recorded by adding 300 scans at the resolution of 4 cm^{-1}.

Computation Procedure

Ab initio molecular orbital (MO) calculations were performed using GAUSSIAN 98[15] on cluster models of DME/Cu(110) explained below. The calculation was performed by using a DFT method at the BLYP level with the 6-31G** basis set, except for the copper atom, for which the Hay-Wadt effective core potential and basis set was used.[16] The equilibrium adsorbate geometry was found by partially optimizing the clusters' total energy while constraining the substrate atoms to the same geometry as that of the bulk state.

Results

Figure 1A,B illustrates the IR spectral changes observed for DME on Ag(110) and p(2 × 1)O−Ag(110) at 80 K with increasing exposures to a monolayer saturation coverage and Figure 2A,B the IR spectral changes observed for DME on Cu(110) and p(2 × 1)O−Cu(110) at 80 K with increasing exposure to monolayer saturation coverage. Parts A and B of Figures3 and 4 exhibit the spectral changes observed for DME-d_6 under the same experimental conditions as those used for the measurements of the spectra in Figures 1 and 2. As explained below, DME and DME-d_6 on all the substrates exhibit distinct spectral changes from those observed at relatively lower exposures to those at higher exposures near a saturation coverage. Tables1 and 2 list the frequencies of IR bands observed at the relatively lower coverages and those at the higher coverages. The stepwise spectral changes with increasing exposures observed for DME and DME-d_6 on the substrates at 80 K were reversed almost completely by the spectral changes observed with increasing the substrate temperature from 80 K to a desorption temperature (ca. 160K); i.e., the spectral features observed near saturation coverages changed to those at lower coverages and then disappeared. These results indicate that the surface structures of Ag(110), Cu(110), p(2 × 1)O−Ag(110), and p(2 × 1)O−Cu(110) are retained during the adsorption and desorption processes of DME and DME-d_6. The frequencies of vibrational bands reported by Levin et al.[10] for DME and DME-d_6 are also listed in the table, together with the assignments proposed by the same authors. (A part of their assignments were revised on the basis of the results of the ab initio MO calculations.) The assignments cannot necessarily be applied to the IR bands of the adsorbates, since the frequencies of the IR bands of DME and DME-d_6 themselves are appreciably different from those of the adsorbates (vide infra).

Infrared Spectra in the 1500−900 cm^{-1} Region Observed for DME on Ag(110), p(2 × 1)O−Ag(110), Cu(110), and p(2 × 1)O−Cu(110). From parts A and B of Figures 1 and 2, it is clear that DME on all the substrates exhibits distinct spectral changes upon increasing exposures. For example, DME on Ag(110) (Figure 1A) at first gives rise to IR bands at 903, 1243, 1450, and 1468 cm^{-1}. On increasing exposures to a saturation coverage level, the 903 cm^{-1} band shifts to 915 cm^{-1}, and new bands appear at 1092, 1167, and 1268 cm^{-1} in addition to the 1243, 1450, and 1468 cm^{-1} bands. As listed in Table 1, the 903 and 1243 cm^{-1} bands are assigned to COC symmetric stretching (ν_s(COC)) and CH_3 rocking ($\rho(CH_3)$) modes, respectively, which belong to the A_1 species. (The adsorbed DME molecule is assumed to have the C_{2v} symmetry as in the case of DME itself.) On the other hand, the 1092 cm^{-1} band can be assigned to a COC asymmetric stretching mode (ν_s(COC)) in the B_1 species and the 1167 cm^{-1} to a $\rho(CH_3)$ mode, which belongs either to B_1 or B_2 species. The 1450 and 1468 cm^{-1} bands can be assigned to CH_3 symmetric deformation ($\delta_s(CH_3)$) and CH_3 asymmetric ($\delta_{as}(CH_3)$) modes, respectively, belonging to the A_1 species. The 1268 cm^{-1} band is tentatively assigned to a $\rho(CH_3)$ mode, which is shifted from the 1243 cm^{-1} band. (The IR band corresponding to the 1268 cm^{-1} band, however, cannot be observed for the adsorbate on Cu(110) and on the reconstructed surfaces. Then the band may be an experimental artifact.) According to the surface selection rule of IRAS,[17] the appearance of the A_1 bands as well as the absence of the B_1 and/or B_2 bands indicates that DME adsorbs on Ag(110) with

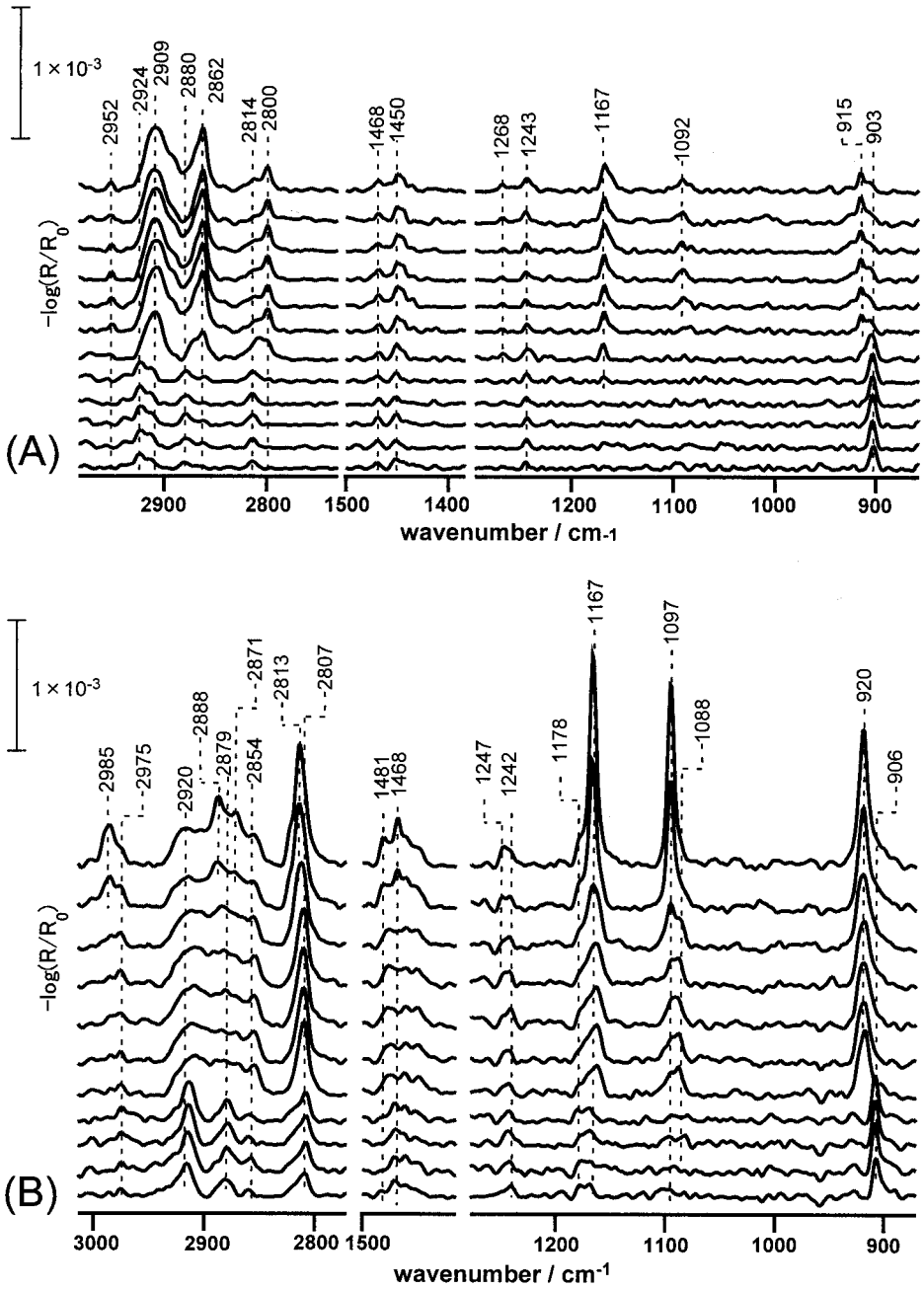

Figure 1. Exposure dependence of the IR spectra of DME on Ag(110) (A) and DME on p(2 × 1)O−Ag(110) (B) measured at 80 K. The vertical lines indicate a scale for the ordinate of each spectrum. The topmost spectra of panels A and B were measured at a nearly saturation coverage level (see text).

the C_2 axis almost perpendicular to the surface at the lower coverages, and the appearance of the IR bands corresponding to the 1092 (B_1) and 1167 (B_1 or B_2) cm^{-1} bands suggests that the adsorbate tilts the axis away from the perpendicular orientation.

The spectral changes observed for DME on Cu(110) (Figure 2A) are quite similar to those observed for the adsorbate on Ag(110). That is, at lower exposures, DME on Cu(110) gives the 895 (ν_s(COC), A_1), 1243 ($\rho(CH_3)$, A_1), 1451($\delta_s(CH_3, A_1)$), and 1464 ($\delta_{as}(CH_3, A_1)$ cm^{-1} bands. Upon increasing exposures, the 895 cm^{-1} band shifts to 901 cm^{-1}, and at the same time, there appear the 1094 (ν_s(COC), B_1) and 1171 ($\rho(CH_3)$, B_1 or B_2) cm^{-1} bands. Thus, DME on Cu(110) undergoes the orientation change from a perpendicular to a tilted one, as in the case of DME on Ag(110). According to Kanazawa and Nukada,[8] DME in the gaseous state gives the ν_s(COC) band at 928 cm^{-1}. The fact that DME on Ag(110) and Cu(110) at the lower exposures gives the corresponding band at the significantly lower frequency side compared to the gaseous sample indicates that the adsorption takes place though coordination of the lone pair electrons in the oxygen atom of DME to the metal surfaces. The red shift of the ν_s(COC) band for DME on Cu(110) ($\Delta\nu = -33$ cm^{-1}) is larger than that for DME on Ag(110) ($\Delta\nu = -25$ cm^{-1}), indicating a stronger coordination of the oxygen atom to Cu(110) compared to the coordination to Ag(110).

The discrete frequency shift of 906 → 920 cm^{-1} for the ν_s(COC) band in Figure 1B and the corresponding shift of 906 → 911 cm^{-1} in Figure 2B suggest that the orientation change of DME takes place also on the reconstructed surfaces, p(2 × 1)O−Ag(110) and p(2 × 1)O−Cu(110). In contrast to the cases of the adsorbate on Ag(110) and Cu(110), however, IR bands

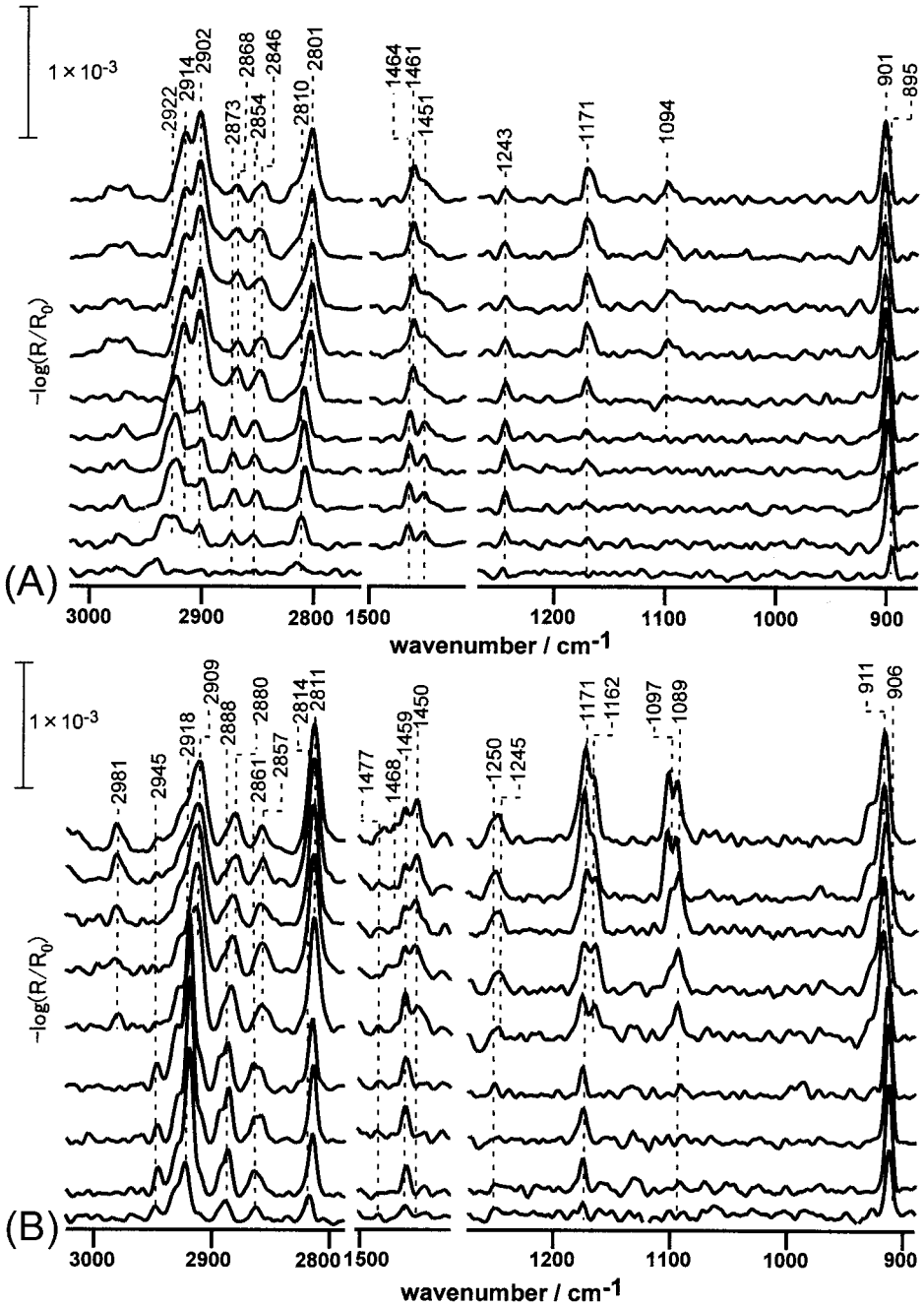

Figure 2. Exposure dependence of the IR spectra of DME on Cu(110) (A) and DME on p(2 × 1)O−Cu(110) (B) measured at 80 K. The vertical lines indicate a scale for the ordinate of each spectrum. The topmost spectra of panels A and B were measured at a nearly saturation coverage level (see text).

ascribable to the ν_s(COC, B_1) and ρ(CH_3, B_1 or B_2) modes can be seen at 1088 and 1178 cm^{-1} in Figure 1B and at 1089 and 1162 cm^{-1} in Figure 2B at lower exposures; the results indicate that the adsorbate on the reconstructed surfaces already takes a more or less tilted orientation relative to the surfaces. Upon increasing the exposures, the ν_s(COC, B_1) and ρ(CH_3, B_1 or B_2) bands show appreciable intensity increase and the following frequency shifts, i.e., 1088 → 1097 cm^{-1} and 1178 → 1167 cm^{-1} in Figure 1B and 1089 → 1097 cm^{-1} and 1171 → 1162 cm^{-1} in Figure 2B. The intensity increase indicates that the C_2 axis tilts further away from the perpendicular direction with increasing exposures. The frequency shifts should be interpreted in terms of weakening in the adsorbate/substrate interaction, because the ν_s(COC, A_1) bands show the shifts to the higher frequency side, indicating the decrease in the coordination of the oxygen atom to the surfaces.

Infrared Spectra in the 3000−2800 cm^{-1} Region Observed for DME on Ag(110), p(2 × 1)O−Ag(110), Cu(110), and p(2 × 1)O−Cu(110). Figure 1A indicates that the IR spectra in the CH_3 stretching vibration region for DME on Ag(110) exhibit distinct changes, which correspond to the orientation change deduced from the spectra in the 1500−900 cm^{-1} region. That is, the adsorbate gives rise to IR bands at 2924, 2880, and 2814 cm^{-1} at lower exposures, and on increasing exposures to a saturation coverage, these bands are replaced by those at 2909, 2862, and 2800 cm^{-1}. Comparison of these spectral changes with those in the corresponding region of Figure 2A indicates that the spectral changes for DME on Cu(110) are considerably

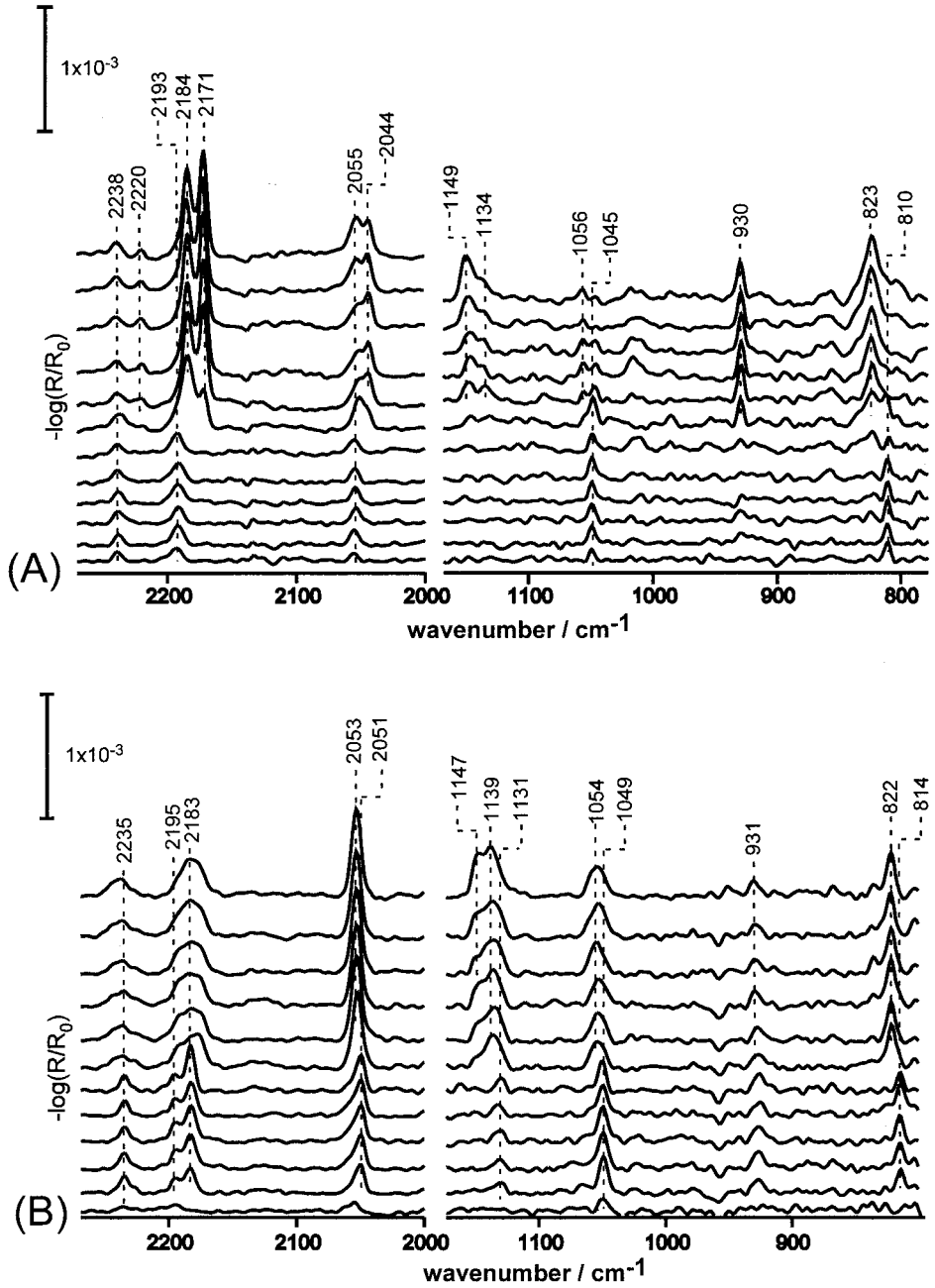

Figure 3. Exposure dependence of the IR spectra of DME-d_6 on Ag(110) (A) and DME-d_6 on p(2 × 1)O−Ag(110) (B) measured at 80 K. The vertical lines indicate a scale for the ordinate of each spectrum. The topmost spectra of panels A and B were measured at a nearly saturation coverage level (see text).

different from those on Ag(110); i.e., at lower exposures the adsorbate on Cu(110) gives IR bands at 2922, 2902, 2873, 2854, and 2810 cm^{-1}, which are replaced by those at 2914, 2902, 2868, 2846, and 2801 cm^{-1} upon increasing exposures to a saturation coverage level. The spectral changes in the CH_3 stretching vibration region observed for DME on p(2 × 1)O−Ag(110) and p(2 × 1)O−Cu(110) (Figures 1B and 2B) are quite different form each other and from those observed for the adsorbate on Ag(110) and Cu(110), although the spectra on the reconstructed surfaces also exhibit stepwise changes corresponding to the orientation change deduced from the spectral changes in the 1500−900 cm^{-1} region.

As shown in Table 1, the symmetric CH_3 stretching vibration ($\nu_s(CH_3)$) in the A_1 species of DME itself appears at 2817 cm^{-1}. The IR bands near 2810 cm^{-1} observed for DME adsorbed on the metal surfaces in Figures 1 and 2 are ascribable to the ν_s-(CH_3, A_1) mode. Upon increasing exposures, the IR band of the adsorbates on Ag(110) and Cu(110) exhibits the frequency shifts of 2814 → 2800 and 2810 → 2801 cm^{-1}, respectively (Figures 1A and 2A), which may be due to increase in the methyl group/substrate interaction associated with the orientation change of the adsorbate. However, the multiplex features of the IR spectra above 2820 cm^{-1} measured especially at the larger exposure levels in Figures 1 and 2 cannot be explained on the basis of the assignments given to DME in Table 1. One of the main reasons for the complicated features is due to Fermi resonances between the fundamental CH_3 stretching modes and the overtones and/or combinations of CH_3 deformation modes of the methyl groups.[18] For adsorbates on metal surfaces, Fermi resonance effects on the vibrational spectra of the methoxy group adsorbed on Mo(110),[19] Al(111), Cu(111),[20] and Cu(100)[21,22] have been studied extensively, indicating that the resonances between the fundamental $\nu_s(CH_3)$ mode and the first overtones of the $\delta_s(CH_3)$ and $\delta_{as}(CH_3)$ of the methoxy group with the C_3

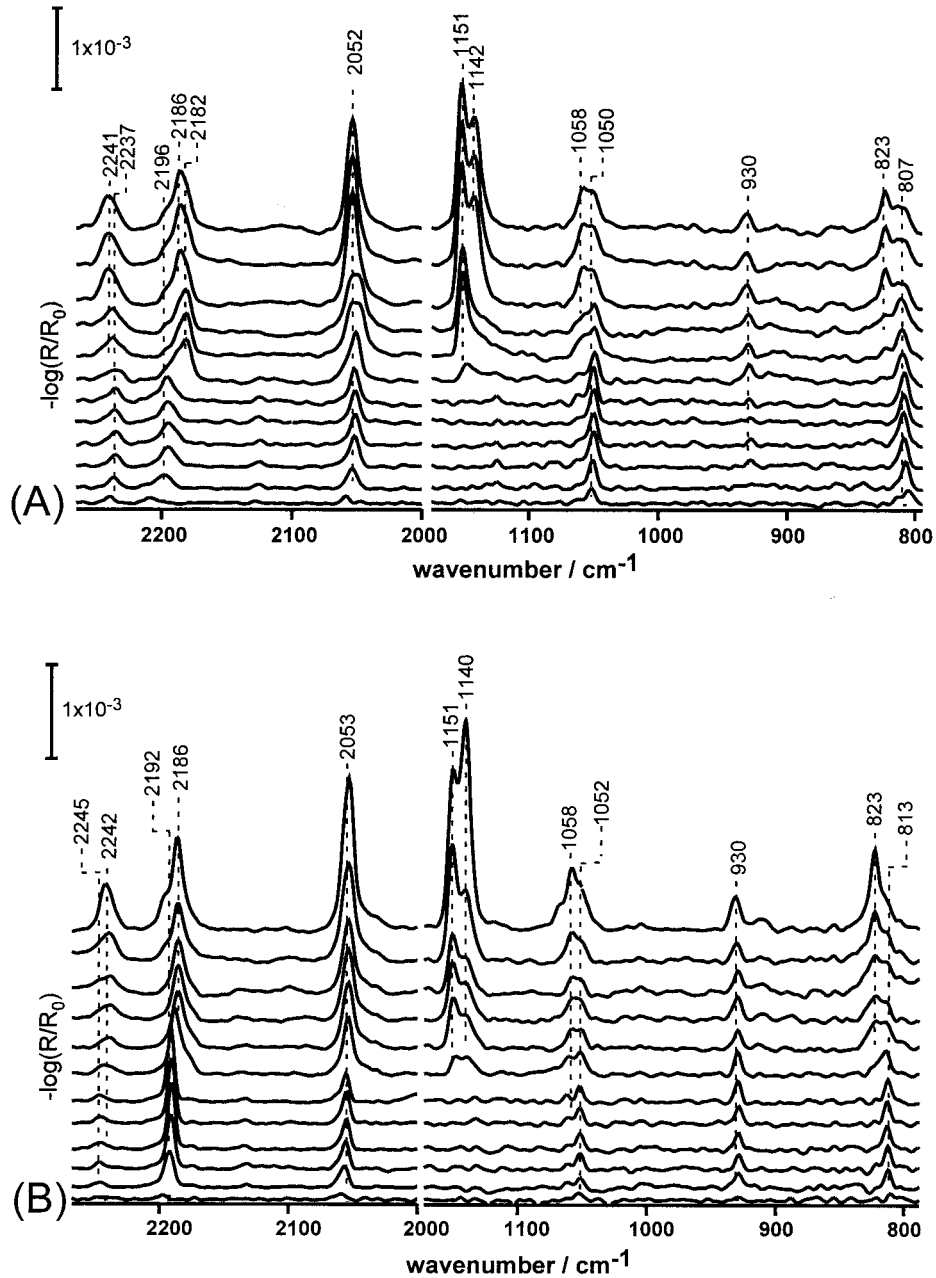

Figure 4. Exposure dependence of the IR spectra of DME-d_6 on Cu(110) (A) and DME-d_6 on p(2 × 1)O−Cu(110) (B) measured at 80 K. The vertical lines indicate a scale for the ordinate of each spectrum. The topmost spectra of panels A and B were measured at a nearly saturation coverage level (see text).

axis perpendicular to the surfaces result in three fairly intense IR bands in the CH_3 stretching vibration region. In the case of DME, there exist two CH_3 stretching modes in the A_1 species ($\nu_s(CH_3)$ and $\nu_{as}(CH_3)$) and six CH_3 deformation modes (δ_{as}-(CH_3, A_1), $\delta_{as}(CH_3, A_1)$, $\delta_{as}(CH_3, B_1)$, $\delta_s(CH_3, B_1)$, $\delta_{as}(CH_3, A_2)$ and $\delta_{as}(CH_3, B_2)$. Then, even if it is assumed that Fermi resonances take place between the fundamental CH_3 stretching modes and the first overtone modes of the deformation vibrations, it may result in very complicated spectral features in the CH_3 stretching vibration region. This result almost hampers our intension to analyze the complicated spectral changes in Figures 1 and 2. Despite this, the marked dependence of the spectral changes on the kind of substrates suggests the existence of subtle changes in the adsorbate/substrate interaction during the orientation transition, which cannot be detected by the spectral changes observed below 1500 cm^{-1}. To elucidate the interaction between the methyl groups and the substrates, the IR spectral changes during the transition were measured for DME-d_6 adsorbed on the substrates. Fermi resonances between the CD_3 stretching fundamental modes and the overtones of the CD_3 deformation modes are expected to be much less than the resonances in the case of DME.

Infrared Spectra in the 1200−800 cm^{-1} Region of DME-d_6 on Ag(110), p(2 × 1)O−Ag(110), Cu(110) and p(2 × 1)-O−Cu(110). Figures 3A and 4A indicate that DME-d_6 on Ag(110) as well as on Cu(110) exhibit clear spectral changes with increasing exposures to a saturation coverage, corroborating the orientation change of the adsorbate inferred from the IR spectra in Figures 1A and 2A. That is, at lower exposures, the adsorbate on both substrates gives rise to an IR band near 810 cm^{-1} due to the $\nu_s(COC, A_1)$ mode, which is shifted from the corresponding IR band near 900 cm^{-1} (in Figures 1A and 1B) with hydrogen/deuterium substitution, and that near 1050 cm^{-1}, which is ascribable either to $\delta_s(CD_3, A_1)$ or to ρ (CD_3, A_1).

TABLE 1: Frequencies (cm^{-1}) and Assignment of IR Bands Observed for DME and DME on the Metal

Ag(110)		p(2 × 1)O−Ag(110)		Cu(110)		p(2 × 1)O-Cu(110)			
low cov.	high conv.	low conv.	high conv.	low conv.	high conv.	low conv.	high conv.	DME[b]	assignment[b]
		2975	2985				2981	2992	CH_3 asym. str. (A_1)
								2987	CH_3 asym. str. (B_1)
				2922	2914	2945			
	2952	2920	2920	2902	2902	2918		2934	CH_3 asym. str. (B_2)
2924	2909	2871	2888					2826	CH_3 asym. str. (B_1)
2880	2862	2854	2852	2873	2968	2888			
				2854	2846	2861			
2814			2813	2810		2814			
	2800	2807			2801		2811	2817	CH_3 sym. str. (A_1)
								1487	CH_3 sym. def. (A_1)
1468	1468			1464		1477	1468	1469	CH_3 sym. def. (B_1)
1450	1450	1468	1468	1451	1462	1459	1459	1464	CH_3 sym. def. (B_2)
	1436						1450	1450	CH_3 sym. def. (B_1)
								1434	CH_3 sym. def. (A_1)
	1268		1247						
1243	1243	1242	1242	1243	1243	1250	1245	1251	CH_3 rock. (A_1)
		1178					1171	1179	CH_3 rock. (B_2)
	1167		1167		1171	1171	1162	1166	CH_3 rock. (B_1)
	1092	1088	1097		1094	1089	1097	1095	C−O−C asym. str. (B_1)
903	915	906	920	895	901	906	911	920	C−O−C sym. str. (A_1)

[a] Frequency values corresponding to low cov. and those to high cov. indicate the observed frequencies measured at low coverages and at high coverages, respectively, of DME on each metal substrate (see text). [b] The observed frequencies and assignments of DME were taken from ref 10.

TABLE 2: Frequencies (cm^{-1}) and Assignment of IR Bands Observed for DME-d_6 and DME-d_6 on the Metal Substrates

Ag(110)		p(2 × 1)O−Ag(110)		Cu(110)		p(2 × 1)O-Cu(110)			
low cov.	high conv.	low conv.	high conv.	low conv.	high conv.	low conv.	high conv.	DME-d_6[b]	assignment[b]
2238	2238	2235		2241	2241		2241	2244	CD_3 asym. str. (A_1)
	2220							2240	CD_3 asym. str. (B_1)
2193		2195		2196		2192		2188	CD_3 asym. str. (B_2)
	2184	2183	2183		2186		2186		
	2171				2182				
2055	2055	2051		2052		2053	2053	2058	CD_3 sym. str. (B_1)
	2044		2053		2052			2053	CD_3 sym. str. (A_1)
1149	1149		1147		1151		1151	1149	COC asym. str. (B_1)
			1139		1142		1140	1136	CD_3 asym. def. (A_1)
	1134	1130							
								1076	CD_3 sym. (A_1)
								1061	CD_3 asym. def. (B_1)
	1056	1049			1058		1058	1054	CD_3 asym. def. (B_2)
1045			1054	1050		1052		1048	CD_3 rock. (A_1)
								1048	CD_3 def. (B_1)
	930	931	931		930	930	930	933	CD_3 rock. (B_2)
	823		822		823		823	824	C−O−C sym. str. (A_1)
810		814		807		813			

[a] Frequency values corresponding to low cov. and those to high cov. indicate the observed frequencies measured at low coverages and at high coverages, respectively, of DME-d_6 on each metal substrate (see text). [b] The observed frequencies and assignments of DME-d_6 were taken from ref 10. A part of the assignments were revised based on the results of the DFT calculation in this paper. (see text)

Upon increasing exposures, the 810 cm^{-1} band shifts to 823 cm^{-1}, and there appear IR bands near 930 and 1055 cm^{-1} and doublet bands near 1150 cm^{-1}. As listed in Table 2, the 930 and 1055 cm^{-1} bands can be assigned to the $\rho(CD_3, B_2)$ and $\delta(CD_3, B_1$ or $B_2)$ modes, respectively, and the 1150 cm^{-1} bands to the $\nu_{as}(COC, B_1)$ mode.

The spectral changes in the 1200−800 cm^{-1} region observed for DME-d_6 on p(2 × 1)O−Ag(110) in Figure 3B are similar to those observed for the adsorbate on p(2 × 1)O−Cu(110) in Figure 4B, and both changes confirm the orientation change proposed to DME on the reconstructed surfaces based on the spectra in Figures 1B and 2B. The $\nu_s(COC, A_1)$ band exhibits discrete frequency change (814 → 822 cm^{-1} in Figure 3B and 813 → 823 cm^{-1} in Figure 4B). The appearance of the 930 cm^{-1} band due to the $\rho(CD_3, B_2)$ mode at lower exposures indicates that the adsorbate takes an orientation with the C_2 axis more or less tilted from the perpendicular orientation. The intensity increase of the $\rho(CD_3, B_2)$ band and appearance of IR bands ascribable to the B_1 and/or B_2 species near 1150 and 1055 cm^{-1} at larger exposures in Figures 3B and 4B indicate that the C_2 axis tilts further away from the perpendicular orientation with increasing exposures.

Infrared Spectra in the CD_3 Stretching Vibration Region of DME-d_6 on Ag(110), p(2 × 1)O−Ag(110), Cu(110), and p(2 × 1)O−Cu(110). As can be recognized from the IR spectra in the 2250−2000 cm^{-1} region of Figures 3 and 4, DME-d_6 on Ag(110), Cu(110), p(2 × 1)O−Ag(110), and p(2 × 1)O−Cu-(110) exhibits distinct changes with increasing exposures. The changes, however, are much simpler than those observed for the CH_3 stretching vibration region of DME on the substrates (Figures 1A and 2A). In addition, DME-d_6 on all the substrates exhibits more or less similar spectral changes, which is also contrasted to the case of the adsorbed DME. These results indicate that Fermi resonance does not give significant effects

on the spectra of DME-d_6. The observed frequencies for the adsorbed DME-d_6 correspond well to those of DME-d_6 itself, which facilitate the assignment of the observed bands (see Table 2). For example, the IR bands at 2238, 2193, and 2055 cm^{-1} observed for DME-d_6 at lower exposures on Ag(110) (Figure 3A) are the counterparts of the 2244, 2188, and 2053 cm^{-1} bands of DME-d_6 itself, which are assigned to the $\nu_{as}(CD_3, A_1)$, $\nu_{as}(CD_3, B_2)$, and $\nu_s(CD_3, A_1)$ modes, respectively. The appearance of the $\nu_{as}(CD_3, B_2)$ band can be explained by considering that at lower exposures the molecular C_2 axis does not take an exactly perpendicular orientation on the surface but a more or less tilted one. As Figure 3A shows, the $\nu_{as}(CD_3, A_1)$, $\nu_{as}(CD_3, B_2)$, and $\nu_s(CD_3, A_1)$ bands split into two bands (2238 and 2220 cm^{-1} for $\nu_{as}(CD_3, A_1)$; 2184 and 2171 cm^{-1} for $\nu_{as}(CD_3, B_2)$; 2055 and 2044 cm^{-1} for $\nu_s(CD_3, A_1)$). Presumably, the methyl groups of the adsorbate with the almost perpendicular orientation state at the lower exposures retain their local C_{3v} symmetry, causing the singlet feature for each mode. On the other hand, upon tilting of the C_2 axis, there occurs an appreciable interaction between the methyl group and the substrate surface, which causes the lowering of the local C_{3v} symmetry. This may be one of the main reasons for the appearance of the doublet bands. Figure 3B indicates that DME-d_6 on p(2 × 1)O−Ag(110) gives doublet bands at 2195 and 2183 cm^{-1} at lower exposures; as already explained, the adsorbate on the reconstructed surface takes a more or less tilted orientation state, corroborating the above-mentioned explanation. DME-d_6 on p(2 × 1)O−Ag(110) at larger exposures give broader bands for the $\nu_{as}(CD_3, A_1)$ and $\nu_{as}(CD_3, B_2)$ modes (see Figure 3B). This may be explained also in terms of the lowering of the local C_{3v} symmetry due to the increased interaction between the methyl groups and the substrate. The spectra observed for DME-d_6 on Cu(110) and p(2 × 1)O−Cu(110) at lower exposures (Figures 4A and 4B) are similar to those the adsorbate on Ag(110), giving singlet bands near 2240, 2195, and 2052 cm^{-1} ascribable to the $\nu_{as}(CD_3, A_1)$, $\nu_{as}(CD_3, B_2)$, and $\nu_s(CD_3, A_1)$ modes. Upon increasing exposures, the 2195 cm^{-1} bands shift to the lower frequency side, and the other bands remain at almost the same positions; in addition, each band does not show any broadening. These results suggest that the interaction mode between the methyl groups and the substrates are different from those on Ag(110) and p(2 × 1)O−Ag(110).

Results of the DFT-MO Calculations on DME and DME-d_6 and Cluster Models of DME and DME-d_6 Adsorbed on Cu(110). As already explained, the appreciable frequency lowering of the $\nu_s(COC, A_1)$ band observed for DME on the substrates suggests that the coordination of the oxygen atom via the lone pair electrons to the Ag and Cu atoms constituting the surfaces plays an important role in the adsorbate/substrate interaction. The coordination interaction should cause frequency shifts on other vibrational modes of the adsorbate, as actually observed in the spectra in Figures 1−4. Thus, the calculation of the normal frequencies of cluster models, where the coordination interaction is properly considered, and the comparison between the observed and calculated frequencies, may give more insight into the adsorbate/substrate interaction. In addition, the determination of the normal frequencies of the CH_3 stretching modes of DME on the substrates, which are not affected by Fermi resonance, is of crucial importance to analyze the complicated spectral features in the CH_3 stretching vibration region of Figures 1 and 2. As a first step of the study along this direction, we performed the normal frequency calculation on the cluster models of DME/Cu(110) shown in panels A and B of Figure 5, which are called LB−Cu(12,6) and SB−Cu(12,6), respectively. The metal substrates in both models have 12 copper atoms in the first layer and six copper atoms in the second layer. DME in the LB−Cu(12,6) model has the oxygen atom coordinated to the neighboring copper atoms in the (001) direction on the (110) surface, while DME in the SB−Cu(12,6) model has the oxygen atom coordinated to the neighboring copper atoms in the (110) direction.

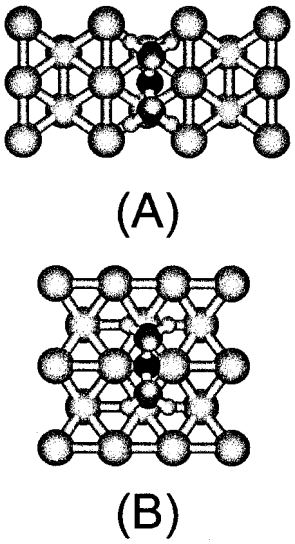

Figure 5. Cluster models of DME/Cu(110): (A) LB−Cu(12,6) and (B) SB−Cu(12,6) (see text).

TABLE 3: Comparison between the Observed and Optimized Structure Parameters of DME and the Optimized Structure Parameters and Adsorption Energy of the Cluster Models

	structural parameters[a]			
	CH_3OCH_3		CH_3OCH_3/Cu(110)	
	obsd.[b]	calcd.	calcd. (I)[c]	calcd. (II)[c]
R(O−Cu) (Å)			2.763	2.331
R(C−O) (Å)	1.410	1.427	1.452	1.468
$R(CH_1)$ (Å)	1.091	1.100	1.101	1.010
$R(CH_2)$ (Å)	1.100	1.110	1.103	1.010
A(COC) (deg)	111.72	111.87	116.03	117.73
$A(OCH_1)$ (deg)	107.23	107.01	111.19	110.02
$A(OCH_2)$ (deg)	110.83	112.03	109.11	108.60
$A(H_2CH_2)$ (deg)	108.73	107.97	108.64	109.19
adsorption energy (kcal/mol)[d]			2.39	7.89

[a] R and A indicate a bond length and a bond angle, respectively. For H_1 and H_2, see text. [b] Data taken from ref 23. [c] The parameters corresponding to calcd. (I) and calcd. (II) are those calculated for the cluster models, LB−Cu(12,6) and SB−Cu(12,6), respectively. [d] The values calculated after the BSSE correction.

The optimized structure parameters of DME itself are listed in Table 3, together with the experimental values.[23] One of the hydrogen atom of each methyl group is assumed to take a trans position with respect to the O−C bond, as experimentally determined.[23] (H_1 in the table denotes the hydrogen atom of the methyl group at the trans position and H_2 the other hydrogen atoms of the same methyl group.) The agreement between the observed and calculated parameters are quite good. The calculated frequencies of DME and DME-d_6 are compared with the observed frequencies in Table 4. The results of calculations well reproduce the observed frequencies, except for those ascribable to CH_3 stretching vibrations. The calculated frequencies for these modes differ from the observed ones by 54−80 cm^{-1}; this is contrasted to the case of the CD_3 stretching vibrations, where the differences between the calculated and

TABLE 4: Comparison between the Observed and Calculated Frequencies (cm^{-1}) for DME, DME-d_6, and the Cluster Models for DME/Cu(110) and DME-d_6/Cu(110)

	CH_3OCH_3		CD_3OCD_3		CH_3OCH_3/Cu(110)			CD_3OCD_3/Cu(110)		
	obsd.[a]	calcd.[b]	obsd.[a]	calcd.[b]	obsd.[b]	calcd. (I)[d]	calcd. (II)[d]	obsd.[c]	calcd. (I)[c]	calcd. (II)[d]
A_1	2992	3046	2244	2257		3035	3072	2241	2252	2282
	2817	2897	2058	2082		2939	2975	2052	2106	2129
	1487	1496	1136	1146	1464	1480	1473		1114	1106
	1434	1461	1076	1071	1451	1468	1465	1050	1071	1067
	1251	1232	1048	1029	1243	1189	1192	(930)	966	965
	920	902	824	808	895	830	802	807	770	746
	425	403	358	339		499	482		429	417
B_1	2987	3045	2240	2253		3032	3067		2251	2279
	2826	2880	2053	2066		2934	2971		2099	2123
	1469	1472	1149	1120		1468	1458		1078	1068
	1450	1431	1061	1064		1420	1427		1069	
	1166	1147	1048	1054	(1171)	1158	1151		1045	1035
	1095	1082	861	846		1028	997		836	826
B_2	2934	2924	2188	2168		3003	3055	(2196)	2229	2269
	1464	1460	1054	1058		1448	1455		1047	1050
	1179	1166	933	920		1119	1115		860	857
	268	243	208	188		204	208		203	207

[a] The observed frequencies are taken from ref 10. [b] The observed frequencies are taken from the spectra observed at lower coverages in Figure 2A. The frequency in the parenthesis is deduced from the spectra measured at higher coverages in Figure 2A. [c] The observed frequencies are taken from the spectra observed at lower coverages in Figure 4A. The frequencies in the parentheses are deduced from the spectra measured at higher coverages in Figure 2A. [d] The frequencies corresponding to calcd. (I) and calcd. (II) are those calculated for the cluster models, LB−Cu(12,6) and SB−Cu(12,6), respectively.

observed frequencies are 24−13 cm^{-1}. These results confirm that the vibrational spectra in the CH_3 stretching vibrations of DME are strongly affected by Fermi resonance.

The optimized geometries for the cluster models, LB−Cu(12,6) and SB−Cu(12,6), are listed in Table 3. In the optimization process, it was assumed that (i) the models keep the C_{2v} symmetry as a whole and (ii) one of the hydrogen atom (denoted by H_1 in the table) takes a cis position retative to the O−C bond because the optimized structures could not be obtained on the assumption of the trans position as in the case of DME. This is due to a strong repulsive interaction between the copper atoms and the H_1 atom taking the trans position. The optimized distances between the oxygen atom and the nearest copper atom are 2.763 Å for LB−Cu(12,6) and 2.331 Å for SB−Cu(12,6), which are well below the sum of the van der Waals radii, 2.92 Å, of the oxygen and copper atoms,[24] indicating the existence of a coordination interaction between the two atoms. The calculated adsorption energy for LB−Cu(12,6) and SB−Cu(12,6) are 2.39 and 7.89 kcal/mol, respectively. Although the cluster size dependence of the optimized structures and the adsorption energy should be tested by extending the calculation to larger cluster models, the present results confirm that the coordination plays an important role in the adsorption of DME to Cu(110). Table 3 indicates that the calculation predicts increase in the CO bond (+0.025 Å for LB−Cu(12,6) and +0.041 Å for SB−Cu(12,6)) as well as the COC angle (+4.16° for LB−Cu(12,6) and +5.86° for SB−Cu(12,6)). The calculated frequencies for both models are listed in Table 4, where the frequencies observed for DME and DME-d_6 on Cu(110) at lower coverages are compared with the calculated ones in the A_1 species. The comparison indicates that the calculated frequencies for both models reproduce well the observed frequencies. From Table 4, it is noticed that the frequency shifts induced by the adsorption observed for the $\nu_{as}(CH_3, A_1)$, $\nu_s(CH_3, A_1)$, $\rho(CH_3, A_1)$, and $\nu_s(COC, A_1)$ bands of DME and the shift observed for the $\nu_s(COC, A_1)$ band of DME-d_6 are as follows; −23, +17, −8, −25, and −14 cm^{-1}. The corresponding calculated shifts are −16, +7, −43, −72, and −38 cm^{-1} for LB−Cu(12,6) and −23, +4, −40, −100, and −62 cm^{-1} for SB−Cu(12,6). The trends of the predicted frequency shifts again correspond well to the observed ones. The frequency shift of the $\nu_s(COC, A_1)$ band is a sensitive probe for the coordination interaction. In this context, the LB−Cu(12,6) model is more favorable than the SB−Cu(12,6) model because the shifts for the former model fit the observed ones better than the shifts for the latter model. As Figure 4A,B shows, DME-d_6 on Cu(110) and on p(2 × 1)O−Cu(110) give rise to prominent IR bands near 1150 cm^{-1} on conversion to the tilted orientation state. Although these bands are tentatively assigned to $\nu_{as}(COC, B_1)$ in the previous section, the results of calculation give any frequency near this region neither to the LB−Cu(12,6) model nor to the SB−Cu(12,6) model. So to get explicit conclusions about the adsorbate/substrate interaction mode in the tilted orientation state, it is necessary to extend the DFT calculations on cluster models for the tilted orientation state.

Conclusions

The IR spectra in the 1500−800 cm^{-1} region observed for DME and DME-d_6 on Ag(110), Cu(110), p(2 × 1)O−Ag(110), and p(2 × 1)O−Cu(110) exhibit distinct changes on increasing exposures to a saturation coverage. The observed changes for DME and DME-d_6 are similar to each other on all the substrates, indicating that the adsorbates undergo a transition from a state with the C_2 axis nearly perpendicular to the surfaces to a state with the axis tilted away from the perpendicular orientation. On the other hand, the IR spectral changes measured in the CH_3 stretching vibration region for DME with increasing exposures to all the substrates, although still exhibiting stepwise changes indicative of the orientation change, strongly depend on the kind of the substrates. This was interpreted in terms of Fermi resonances between the fundamental CH_3 stretching modes and the overtone and/or combination modes of the CH_3 deformation modes of the methyl groups. On conversion from the almost perpendicular orientation state to the tilted one, there should occur frequency changes in the normal modes of the CH_3 stretching and CH_3 deformation. Even if the latter frequency changes and their dependence on the kind of substrates cannot be detected within the limits of detection and accuracy of the apparatus used for the measurements (as shown in the Experi-

mental Section, the resolution of the spectrometer is 4 cm^{-1}), the frequency changes are enhanced through the resonance effects, resulting in the large spectral changes in the CH_3 stretching vibration region. Thus, the IR bands in the CH_3 stretching vibration region of DME on the substrates indicate the existence of subtle difference in the adsorbate/substrate interactions, although explicit explanations to the differences have not been given yet.

The substantial frequency lowering of the ν_s(COC, A_1) band observed for the almost perpendicular orientation state relative to the corresponding frequency of the gaseous sample (−25 (DME) and −17 cm^{-1} (DME-d_6) for the adsorbates on Ag(110) and −33(DME) and −20 cm^{-1}(DME-d_6) for the adsorbates on Cu(110)) indicates the coordination interaction of the oxygen of DME to the substrate silver and copper atoms. DFT calculations were carried out on the models, LB−Cu(12,6) and SB−Cu(12,6), shown in Figure 5, where the metal surfaces are modeled by the clusters consisting of 12 copper atoms in the first layer and six atoms in the second layer and DME adsorbs to the surfaces with the oxygen atom coordinating to neighboring two copper atoms. The results of calculations reasonably well reproduce the frequencies of IR bands observed for DME and DME-d_6 on Cu(110), corroborating the interaction through the coordination of the oxygen to the copper atoms of the surface. Comparing the calculated adsorption frequency shifts of IR bands of DME and DME-d_6 on Cu(110) with the observed frequency shifts, the LB−Cu(12,6) model seems to be more favorable than the SB−Cu(12,6) model because the predicted shifts for the former model fits to the observed ones better than those for the latter. This conclusion, however, does not correspond to the calculated adsorption energy, since the energy (2.39 kcal/mol) for LB−Cu(12,6) is less than the energy (7.89 kcal/mol) for SB−Cu(12,6). Thus, to get more explicit conclusions about the adsorption modes of DME, DFT calculations should be extended further by using larger cluster models with various adsorption sites. Despite these facts, the results of calculations prove that the normal frequency calculation based on DFT is one of the efficient methods to analyze the IR spectra of adsorbates on metal surfaces, where relatively weak interaction forces play dominant roles as in the systems treated by the present paper.

References and Notes

(1) Chabal, Y. J. *Surf. Sci. Rep*. **1988**, *8*, 211.

(2) Bradshow, A. M.; Schweizer, E. In *Spectroscopy of Surfaces*; Clark, R. J. H., Hester, R. E., Eds.; John Wily & Sons Ltd.: New York, 1988; p 413.

(3) Trenary, M. *Annu. Rev. Phys. Chem*. **2000**, *51*, 381.

(4) Akita, M.; Osaka, N.; Itoh, K. *Surf. Sci.* **1998**, *405*, 172.

(5) Osaka, N.; Akita, M.; Itoh, K. *J. Phys. Chem.* **1998**, *102*, 6817.

(6) Osaka, N.; Akita, M.; Hiramoto, S.; Itoh, K. *Surf. Sci.* **1999**,*427/428*, 381.

(7) Akita, M.; Hiramoto, S.; Osaka, N.; Itoh, K. *J. Phys. Chem.* **1999**, *103*, 10189.

(8) Kanazawa, Y.; Nukada, K. *Bull. Chem. Soc. Jpn.* **1962**, *35*, 612.

(9) Allan, A.; McKean, D. C.; Perchard, J.-P.; Josien, M.-L. *Spectrochim. Acta* **1971**, *27A*, 1409.

(10) Levin, I. W.; Pearce, R. A. R.; Spiker, R. C., Jr. *J. Chem. Phys*. **1978**, *68*, 3471.

(11) McKean, D. C.; Kindness, A.; Wilkie, N.; Murphy, W. F. *Spectrochim. Acta* **1996**, *52A*, 445.

(12) Sexton, B. A.; Hughes, A. E. *Surf. Sci.* **1984**, *140*, 227.

(13) Ng, L.; Chen, J. G.; Basu, P.; Yates, J. T. Jr. *Langmuir* **1987**, *3*, 1161.

(14) Bugyi, L.; Solymosi, F. *Surf. Sci.* **1997**, *385*, 365.

(15) Frisch, M. J.; Trucks, G. W.; Schlegel, H. B.; Scuseria, G. E.; Robb, M. A.; Cheeseman, J. R.; Zakrzewski, V. G.; Montgomery, J. A.; Stratmann, R. E.; Burant, J. C.; Dapprich, S.; Millam, J. M.; Daniels, A. D.; Kudin, K. N.; Strain, M. C.; Farkas, O.; Tomasi, J.; Barone, V.; Cossi, M.; Cammi, R.; Mennucci, B.; Pomelli, C.; Adamo, C.; Clifford, S.; Ochterski, J.; Petersson, G. A.; Ayala, P. Y.; Cui, Q.; Morokuma, K.; Malick, D. K.; Rabuck, A. D.; Raghavachari, K.; Foresman, J. B.; Cioslowski, J.; Ortiz, J. V.; Stefanov, B. B.; Liu, G.; Liashenko, A.; Piskorz, P.; Komaromi, I.; Gomperts, R.; Martin, R. L.; Fox, D. J.; Keith, T.; Al-Laham, M. A.; Peng, C. Y.; Nanayakkara, A.; Gonzalez, C.; Challacombe, M.; Gill, P. M. W.; Johnson, B. G.; Chen, W.; Wong, M. W.; Andres, J. L.; Head-Gordon, M.; Replogle, E. S.; Pople, J. A. Gaussian 98, Revision A.9; Gaussian, Inc.: Pittsburgh, PA, 1998.

(16) Hay, P. J.; Wadt, W. R. *J. Chem. Phys.* **1985**, *82*, 284.

(17) Greenler, G. R. *J. Chem. Phys*. **1966**, *44*, 310

(18) Uvdal, P.; Weldon, M. K.; Friend, C. M. *Phys. Rev.* **1994**, *B50*, 12258.

(19) Weldon, M. K.; Friend, C. M. *Chem. Rev.* **1996**, *96*, 1391.

(20) Head, J. D.; Shi, Y. *Int. J. Quantum Chem.* **1999**, *75*, 815.

(21) Asmundsson R.; Uvdal, P. *J. Chem. Phys*. **2000**, *112*, 366.

(22) Mudalige, K.; Trenary, M. *J. Phys. Chem. B* **2001**, *105*, 3823.

(23) Blukis, U.; Kasai, P. H.; Myers, R. J. *J. Chem. Phys.* **1963**, *38*, 2753.

(24) Bondi, A. *J. Phys. Chem*. **1964**, *68*, 441.